Structural Durability &
Health Monitoring

Tech Science Press

https://doi.org/10.32604/sdhm.2026.083367

ARTICLE

A Study on the Fatigue Failure Characteristics of Steel Bridge Deck Pavement Layers under Dynamic Loads

Jiyi Li[1], **Zongqi Xiong**[2] **and Xinxin Cao**[3,*]

[1]Chongqing Highway Maintenance Engineering (Group) Co., Ltd., Chongqing, China
[2]JSTI Chongqing Inspection, Testing and Certification Co., Ltd., Chongqing, China
[3]Department of Road and Urban Railway Engineering, Beijing University of Technology, Beijing, China

*Corresponding Author: Xinxin Cao. Email: caoxinxin@sdut.edu.cn

Received: 02 April 2026; Accepted: 20 May 2026; Published: 24 August 2026

ABSTRACT: In response to the common interlaminar shear and delamination defects in the pavement of long-span steel bridges, this paper investigates the interface fatigue failure mechanism of the "SMA-13 + epoxy resin + orthotropic steel plate" system. Static direct shear tests indicate that the optimal application rate of epoxy resin is 1.5 kg/m^2, and that elevated temperatures cause the failure mode to transition from brittle fracture to ductile creep. Based on full-factorial dynamic shear fatigue tests, this study discarded subjective empirical thresholds and innovatively proposed the "geometric tangent method" to quantitatively define fatigue life. Analysis of variance (ANOVA) revealed that the sensitivity of each factor to fatigue life, in descending order, is: temperature > loading frequency > stress level. Consequently, this study developed a high-precision, multifactorial life prediction model (R^2 = 0.962), providing a scientific basis for evaluating the long-term service performance of bridge decks. Further validation using experimental data is required.

KEYWORDS: Steel bridge deck surfacing; interfacial shear fatigue; epoxy resin; damage progression; service life prediction model

1 Introduction

Orthotropic steel bridge decks (OSBD) have found extremely widespread application in modern bridge engineering projects worldwide, such as long-span suspension bridges and cable-stayed bridges, owing to their significant technical advantages, including low self-weight, high ultimate load-bearing capacity, appropriate overall stiffness, and suitability for factory prefabrication and assembly [1–4]. However, due to the unique structural characteristics of orthotropic steel deck systems, the deck slab is typically relatively thin (usually 14–16 mm), resulting in significant local deflection when heavy vehicles pass over it [5]. At the same time, steel plates have an extremely high thermal conductivity, which means the asphalt concrete pavement laid directly on top of them is subjected to severe mechanical interactions, significant long-term temperature fluctuations, and high-frequency dynamic wheel loads [6,7]. In extremely complex service environments, steel bridge deck pavements must possess excellent resistance to rutting at high temperatures, resistance to cracking at low temperatures, and outstanding interlayer fatigue resistance. Extensive engineering practice and investigations into pavement defects have shown that interlayer shear failure-such as pavement displacement, rutting, cracking and extensive delamination, has become one of the most common and critical early-stage defects limiting the long-term service life of large-span steel bridge deck pavements [8,9]. Once the bond between the deck and the steel deck fails, the system, which was originally designed to bear loads as a composite structure, will degrade into separate load-bearing units. This not only leads to severe secondary stress concentrations within the deck, thereby inducing fatigue cracking, but also allows rainwater to penetrate the interface, causing severe corrosion of the underlying steel deck. Ultimately, this significantly shortens the overall structural life of the bridge and results in extremely high maintenance and repair costs [10–12].

In order to effectively resist the enormous horizontal shear stresses generated beneath the pavement surface during vehicle braking, acceleration and overloading, the selection and performance optimisation of the interlayer bonding material (tack coat/bonding layer) are of paramount importance. The interlayer bonding system serves as the core 'mechanical link' connecting the rigid steel bridge deck to the flexible asphalt concrete pavement. It must not only provide extremely high shear and pull-out strength, but also remain stable under the high temperatures encountered during pavement construction and demonstrate excellent fatigue resistance across the wide temperature range encountered during the bridge's service life [13,14]. Currently, epoxy resin and its modified systems have become the material of choice for interlayer bonding in the deck surfacing of long-span steel bridges both domestically and internationally, owing to the ultra-high mechanical strength, exceptional high-temperature thermal stability, strong physicochemical adsorption at interfaces, and excellent compatibility with asphalt mixtures afforded by their three-dimensional cross-linked network structure [15–18]. Research indicates that the use of high-performance two-component epoxy resin as a bonding layer can significantly enhance the mechanical interlocking and chemical adhesion between coarse steel plates and discontinuously graded materials such as SMA (asphalt mastic aggregate) [19–21].

Although extensive research has been conducted into the mechanical properties of epoxy adhesive systems, numerous scholars have used static direct shear tests and pull-off tests to investigate in depth the effects of ambient temperature, the roughness of the steel plate surface following rust removal, the interval time, and the amount of adhesive applied on the ultimate interfacial load-bearing capacity [9,22]. However, static shear strength merely represents the mechanical properties of a material under a single ultimate failure condition. It cannot accurately reflect the long-term stress evolution of the pavement interface under actual traffic loads. In real-world bridge deck service conditions, the interface is subjected to repetitive, high-frequency dynamic pulse shear stresses with specific waveforms generated by loaded vehicles [23]. Both asphalt mixtures and epoxy bonding layers exhibit strong viscoelastic properties, and their dynamic mechanical response and damage accumulation rate are highly dependent on ambient temperature and loading frequency [24–27].

Under dynamic loading, failure within the pavement layers of steel bridges is a progressive, cumulative fatigue process involving the initiation of micro-damage, the propagation of macro-cracks, and ultimately interface instability. The coupled effects of varying ambient temperatures (such as extreme summer heat and severe winter cold), different vehicle speeds (such as high-speed driving and low-speed congestion), and varying wheel load intensities (such as standard axle loads and severe overloading) result in the interlayer shear fatigue behaviour exhibiting a high degree of non-linearity and complexity [28]. In recent years, some researchers have begun to utilise hydraulic servo testing systems to investigate interlaminar shear fatigue, confirming that the evolution of fatigue damage at interfaces exhibits a typical 'three-stage' pattern: an initial stage of micro-damage compaction, a stable linear growth stage, and a subsequent stage of accelerated failure [29]. In the data processing and service life evaluation system for dynamic shear fatigue testing, how to define the fatigue life (N_f) of an interface scientifically and objectively has long been a challenging issue in academic circles. Traditional fatigue evaluation of pavement materials typically employs either a reduction in the modulus of stiffness to 50% of its initial value or the setting of an empirical absolute displacement threshold as a failure criterion [30]. However, when testing the shear deformation of steel-asphalt composite interfaces with high viscoelasticity, these traditional guidelines are highly susceptible to interference from high-frequency noise in the testing system and the high-temperature rheological properties of the material. This results in highly subjective and poorly reproducible life assessment outcomes, making it impossible to accurately identify the true physical critical point at which the interface stiffness transitions from linear, stable decay to non-linear macroscopic instability.

In view of the research background previously outlined and the shortcomings of extant evaluation systems, this study conducted an in-depth investigation into the interlaminar shear fatigue failure behaviour of typical long-span steel bridge deck systems. In recent years, prominent scholars have conducted in-depth research into the mechanisms by which dynamic loads impact the fatigue life of pavement structures, offering valuable insights for the research approach of this paper. The central tenets of this study are as follows: Firstly, it abandons traditional empirical failure criteria, which are susceptible to environmental interference, and introduces the geometric tangent method, which possesses clear geometric, mathematical, and physical-mechanical significance. Furthermore, it establishes strict quantitative criteria for selecting the linear fitting interval for the first time, thereby scientifically and objectively defining the fatigue life, N_f, of the interface. Secondly, it not only qualitatively analyses the combined influence of temperature, vehicle speed, and load intensity on the damage evolution rate, but also establishes a mathematical model for predicting the interlayer shear fatigue life based on extensive experimental data, accounting for multivariate coupling.

2 Test Materials and Methods

2.1 Test Materials and Specimen Preparation

To simulate a standard steel bridge deck pavement system, the layers, from top to bottom, consisted of a 5 cm-thick SMA-13 asphalt mixture, an epoxy-resin bonding course and a 4 cm-thick orthotropic steel bridge deck slab. The binder-to-aggregate ratio of the SMA-13 asphalt mixture was 6.0%, with SBS-modified bitumen used; the specific physical properties of the bitumen are shown in Table 1. Table 2 showed the gradation range of the SMA-13 mixture; 0.3% (by mass) of lignin fibre had been added, and the void ratio of the laboratory-moulded specimens was 3.2%.

Table 1: Technical specifications for the three key parameters of SBS-modified Bitumen (Grade I–D).

Technical Indicators	Unit	Standard Requirements	Test Results	Test Method
Penetration (25°C, 100 g, 5 s)	0.1 mm	40~60	51	T 0604
Duration (5°C, 5 cm/min)	cm	≥20	32	T 0605
Softening point (ring method)	°C	≥60	75	T 0606

Table 2: Design gradation ranges for SMA-13 asphalt mixture.

Mesh Size (mm)	16	13.2	9.5	4.75	2.36	1.18	0.6	0.3	0.15	0.075
Specified pass rate range (%)	100	90–100	50–75	20–34	15–26	14–22	12–18	10–15	9–14	8–12
Recommended design targets (%)	100	95	62.5	27	20.5	18	15	12.5	11.5	10

The surface of a 10 mm thick steel plate was sandblasted to remove rust and achieve a Sa 2.5 surface roughness grade to enhance mechanical interlocking. A two-component epoxy resin was uniformly sprayed at gradients of 1.0, 1.25, 1.5, 1.75, and 2.0 kg/m^2 under ambient conditions of 25°C (see Table 3 for technical specifications). Before the adhesive reached the initial setting stage, SMA-13 mix preheated to 170°C was spread over the steel plate and compacted using a wheel-trace forming machine to ensure optimal chemical adhesion and physical interlocking between the layers. Finally, use a precision cutting machine to cut the large specimen into composite test specimens measuring 100 mm × 100 mm × 90 mm, as illustrated in Fig. 1.

Table 3: Key technical specifications of epoxy resin adhesives.

Test Items	Unit	Technical Specifications	Typical Test Results	Test Method
Tensile strength (23°C)	MPa	≥15.0	18.5	GB/T 2567
Elongation at break (23°C)	%	≥30.0	45	GB/T 2567
Compared to the tensile strength of steel plates (23°C)	MPa	≥6.0	8.2	ASTM D4541
Validity period (25°C)	min	≥30	45	GB/T 7123
Viscosity (25°C, after mixing)	Pa·s	0.5~2.5	1.2	T 0625

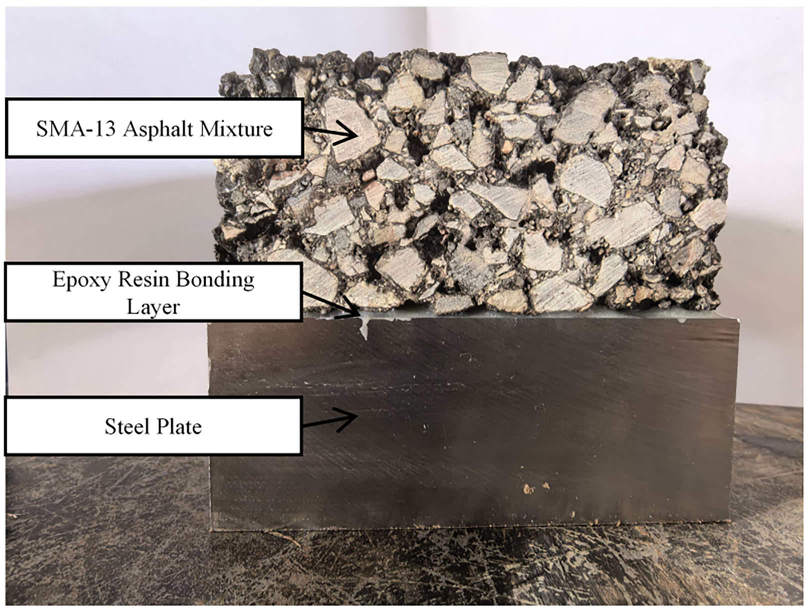

Figure 1: Test specimen for shear testing.

2.2 Static Shear Test

To evaluate the ultimate shear strength of the 'SMA-13 + epoxy resin + steel plate' pavement system under extreme environmental conditions, this study employed a universal testing machine to conduct static direct shear tests. The experimental tests were conducted under strictly controlled ambient temperatures, set at 10°C (simulating winter), 25°C (ambient temperature) and 40°C (simulating high summer temperatures). Before loading, the test specimen must be placed in a climate chamber for a period of four hours of temperature-controlled curing in order to ensure a uniform internal temperature distribution. To eliminate errors caused by differences in thermal conductivity between different material layers, a specially fabricated dummy specimen with an embedded thermocouple was used for the test. Real-time monitoring confirmed that, after a period of four hours, both the interface and the core of the composite material had reached the target temperatures. The test employed a displacement-controlled loading mode, with the loading rate set at 50 mm/min. The selection of this rate was undertaken in accordance with the prevailing provisions for mechanical testing of asphaltic materials, as delineated in the standard (JTG E20-2011), to approximate quasi-static conditions with the greatest possible fidelity while circumventing the undue discrete rheological behaviour engendered by the viscoelastic nature of asphalt under conditions of low-speed loading. In consideration of the pronounced viscoelastic characteristics exhibited at the polymer interface, the resultant measured shear strength manifests a discernible degree of rate dependence. The test was terminated when the shear force reached its peak and then dropped significantly. The peak load, P_{max}, was recorded, and the static shear strength, τ_s, shall be calculated using the formula $\tau_s = P_{max}/A$ (where A is the effective cross-sectional area of the shear interface). Each set of test conditions was repeated three times in parallel, and the arithmetic mean was taken as the subsequent reference value.

2.3 Dynamic Shear Fatigue Testing

Throughout its service life, the deck of a steel bridge is subjected to repeated impacts from traffic loads. Interlaminar failure typically manifests as a process of fatigue damage progression. A UTM-25 servo testing machine was used to apply continuous half-sine wave loading to simulate dynamic vehicle loads. During loading, the stress-controlled mode was maintained, with three stress levels set at 0.15, 0.30, and 0.45, respectively. Additionally, to account for differences in vehicle speed, dynamic fatigue shear tests were conducted at frequencies of 0.1, 1, and 10 Hz. The fatigue life N_f was determined using the geometric tangent method: To eliminate subjective bias, the cumulative life range from 20% to 60% (with $R^2 \geq 0.95$) was selected as the steady-state growth phase (Stage 2), and the data from the final 10% before failure was treated as the accelerated failure phase (Stage 3) for linear regression; N_f was determined by the intersection of the two straight lines. For each test condition, three parallel specimens are prepared to ensure data reliability, and their average value is taken as the final fatigue life N_f. If the dispersion of a single set of data exceeds 15%, additional tests are conducted.

3 Results and Discussion

3.1 The Effect of Temperature on Static Mechanical Properties

This study utilised a series of static direct shear tests to meticulously analyse the interplay between ambient temperature and adhesive application volume on the shear strength of the SMA-13 + epoxy resin + steel plate interface. As illustrated in Fig. 2, the mean interlaminar shear strength of the steel bridge deck paving system exhibits variation according to the amount of epoxy resin sprayed, at ambient temperatures of 10°C, 25°C and 40°C. As demonstrated in Fig. 2, an increase in the quantity of resin that is sprayed results in a parabolic trend in the interlaminar shear strength, which initially increases and then decreases. When the coating weight reached 1.50 kg/m^2, the interfacial shear strength reached its maximum peak; as the temperature increased from 10°C to 40°C, the peak shear strength decreased from 5.4 to 3.8 MPa and then to 1.6 MPa, representing a 70.3% reduction in peak shear strength as the temperature rose. This is due to the fact that, when the application rate is low (1.00–1.25 kg/m^2), the epoxy resin adhesive is unable to fill the voids between the micro-protrusions on the surface of the orthotropic steel plate and the pores at the base of the SMA-13. This results in an insufficient effective bonding area. On a macroscopic level, this is evident in limited shear strength, with the predominant failure mode being adhesive failure. However, when the application rate exceeds a critical threshold (>1.50 kg/m^2), excess resin accumulates at the interface, forming a relatively thick lubricating resin film. As the cohesive strength within the thick resin layer is lower than its adhesive strength to the substrate, under shear loading, the failure mode shifts from interfacial debonding to cohesive failure within the adhesive. This weakens the mechanical interlocking effect between the SMA-13 and the steel plate. Consequently, this study determined that 1.5 kg/m^2 is the optimal dosage of bonding agent and used this as the reference condition for subsequent static and dynamic mechanical evaluations.

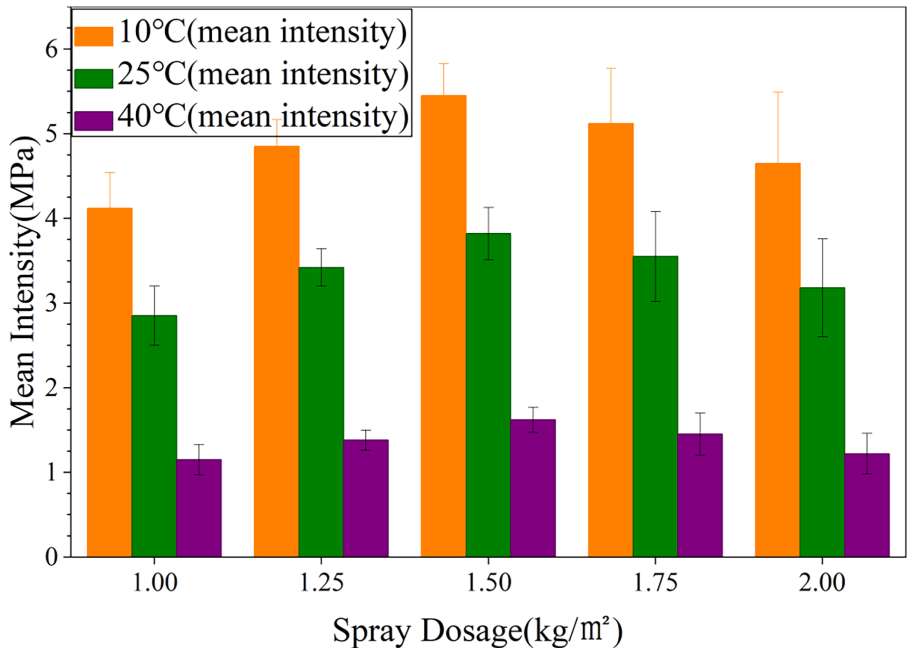

Figure 2: Relationship between epoxy resin application rate and shear strength at different temperatures.

The optimal spraying process parameter, as determined by the researchers, was found to be 1.50 kg/m^2. Fig. 3 then goes on to analyse the static shear force-displacement constitutive response curve of the interface in this pavement system under different temperature fields. The shape of this curve accurately captures the initial stiffness, damage evolution and ultimate deformation capacity of the interface during the shear failure process. The study established that an increase in ambient temperature resulted in a decline in load-bearing capacity and a fundamental shift in the interface failure mode. At a low temperature of 10°C, the initial slope of the shear force–displacement curve reached its maximum; the shear stress exhibited a steep increase in a near-linear fashion with displacement, and the peak load reached 55 kN at a very small displacement of 1.5 mm, followed by a marked brittle drop. This indicates that at 10°C, both the bituminous mortar and the epoxy resin in SMA-13 are in a glassy, hard and brittle state; the interface lacks the capacity for buffering deformation, the energy dissipation rate is extremely low, and typical brittle fracture characteristics are exhibited. When the temperature rises to 25°C, the initial shear stiffness of the system exhibits a structural decline, and the peak corresponding to the ultimate displacement is delayed to the range of 1.8–2.0 mm; subsequently, the curve displays a gentler softening branch. This finding signifies a transition from elastic to plastic behaviour within the material, with interfacial cracks demonstrating steady-state propagation. This is observable macroscopically as elasto-plastic failure. In conditions of elevated temperature (40°C), there is a substantial deterioration in interfacial shear stiffness, resulting in a significant reduction in maximum shear force to approximately 16 kN. Upon reaching the critical load, no distinct stress-unloading phase was observed; instead, a low-level yield plateau was maintained across a very wide displacement range (2.0–3.0 mm and above). This phenomenon is attributed to the softening and flow of the asphalt binder under extremely high-temperature conditions during the summer months. Consequently, the viscous damping characteristics of the epoxy interface layer become the predominant factor in the mechanical response of the system, resulting in a complete shift in failure mode to viscoplastic flow failure. Consequently, when designing steel bridge deck pavements for long-term service, it is essential to assess the risk of interface failure on a case-by-case basis, taking into account the characteristics of the temperature field across different seasons.

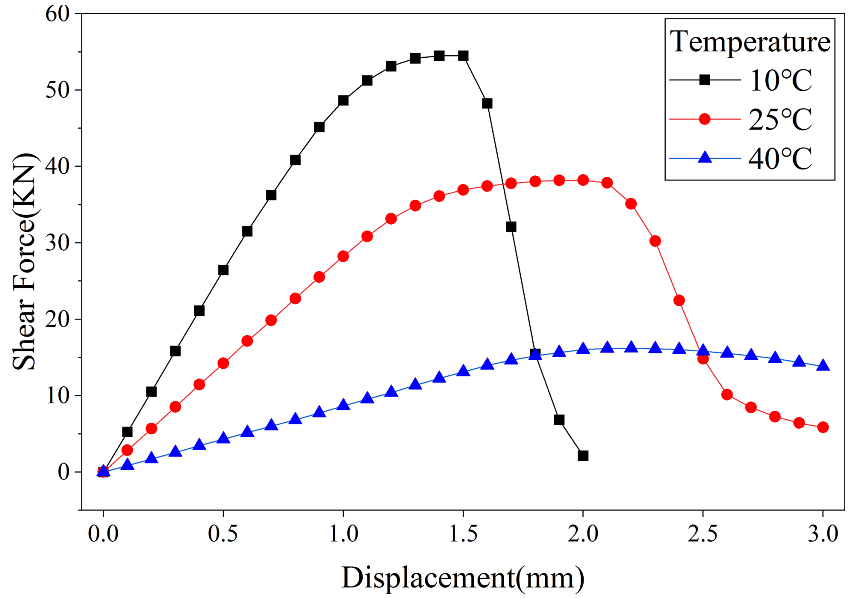

Figure 3: Static shear force-displacement constitutive response curves under different temperature fields.

3.2 Patterns of Dynamic Interlayer Shear Fatigue Displacement Evolution

The purpose of this section is to elucidate the dynamic fatigue damage mechanisms of steel bridge deck pavement systems under real traffic loads. To this end, full-factor dynamic shear fatigue tests were conducted under constant stress control, based on the optimal epoxy resin dosage of 1.50 kg/m^2, as determined in previous studies. As illustrated in Fig. 4, the complete evolution of the interlaminar cumulative shear displacement, designated as δ, is shown as a function of the number of loading cycles, N, under typical operating conditions of 25°C, 0.3 SSR and 1 Hz. As demonstrated in Fig. 4, the interfacial fatigue deformation displays a distinctive 'three-stage' non-linear response. The initial loading phase, accounting for approximately 5%–10% of the total service life, was characterised by a rapid increase in cumulative displacement, which subsequently decelerates. The deformation observed during this stage was attributed to the secondary compaction of pores within the SMA-13 composite mixture, as well as the closure of initial microdefects in the epoxy resin interface layer and the redistribution of stresses. The second stage was characterised by the stable propagation of damage, during which the cumulative displacement increased at a slow, nearly linear and uniform rate with the number of loading cycles. In this stage, interfacial microcracks propagated in a steady state driven by shear stress, and the system remained in a dynamic equilibrium between energy dissipation and stiffness degradation. The slope (rate of displacement increase) in this stage directly reflected the material's ability to resist fatigue damage. The third stage was the accelerated failure phase. Once the cumulative damage exceeded a critical threshold, displacement undergoes a sudden change and rises sharply on an exponential curve. This finding was indicative of significant debonding and through-shear slippage at the interface, which had resulted in the loss of load-bearing capacity of the pavement layer.

In the third stage, displacement diverges rapidly, which makes it extremely difficult in engineering practice to pinpoint the exact point of fracture. Consequently, this study employs the internationally recognised Geometric Tangent Method, which involves performing linear fitting on the stable segment of the second stage and the acceleration segment of the third stage, respectively. The number of cyclic loading cycles corresponding to the intersection point of the two tangents is defined as the interlaminar shear fatigue life N_f of the system. This method effectively eliminates the interference caused by instability in the later stages of the test, thereby laying a reliable data foundation for the subsequent development of high-precision life prediction models.

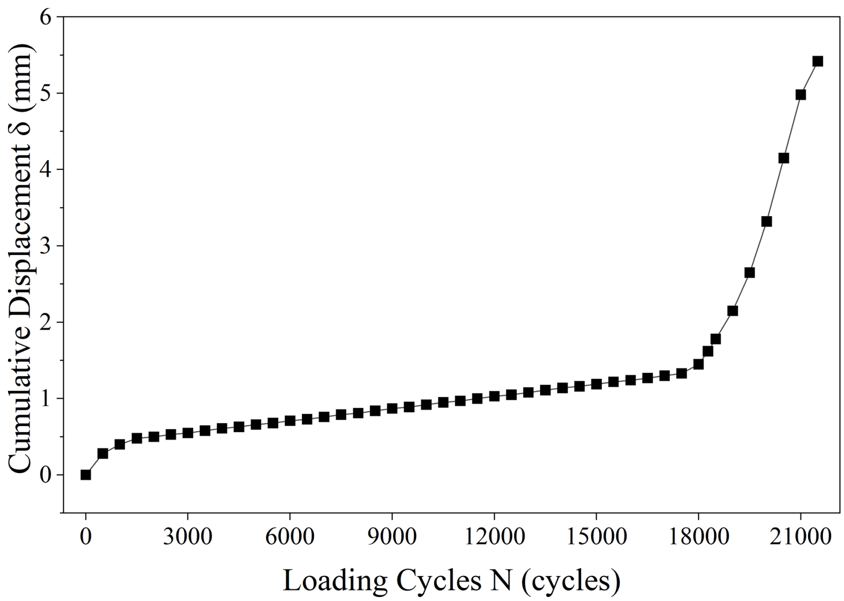

Figure 4: The entire evolution of the cumulative interlaminar shear displacement δ as a function of the number of loading cycles N under typical operating conditions of 25°C, 0.3 SSR and 1 Hz.

3.3 *The Effect of Multifactorial Coupling on the Characteristics of Dynamic Interlaminar Shear Deformation and Fatigue Life*

It is imperative to acknowledge that, throughout the duration of the service life of long-span steel bridges, the pavement system is subjected to a combination of complex, alternating and coupled effects, which are a direct result of ambient temperature, loading frequency and stress levels. To comprehensively elucidate the fatigue failure limits of this system, this study conducted full-factorial orthogonal dynamic shear tests covering a wide temperature range (10°C, 25°C, 40°C), multiple frequencies (0.1, 1, 10 Hz) and multiple stress levels (0.15, 0.30, 0.45 SSR).

3.3.1 Macro-Coupled Response of Fatigue Life under All Factors

As illustrated in Table 4, the interlaminar shear fatigue life, N_f, has been determined for 27 sets of orthogonal test conditions. The experimental findings demonstrated that, under optimal conditions (10°C, 10 Hz, 0.15 SSR), the system's fatigue life reached a maximum of 145,800 cycles. Conversely, under the most challenging conditions (40°C, 0.1 Hz, 0.45 SSR), the life diminished significantly to 120 cycles. The observed discrepancy suggested that the fatigue failure occurring at the pavement interface was not attributable to a single factor. Instead, it manifests as a pronounced non-linear, multi-factor coupled degradation characteristic.

Table 4: Summary of fatigue life (N_f) from full-factorial experiments.

No.	Temperature T (°C)	Frequency f (Hz)	Stress Ratio SSR	Fatigue Life N_f (Cycles)	Standard Deviation σ
1	10	10	0.15	145,800	7290
2	10	10	0.3	82,400	4944
3	10	10	0.45	32,300	2584
4	10	1	0.15	92,500	5550
5	10	1	0.3	58,420	4089
6	10	1	0.45	18,200	1638
7	10	0.1	0.15	24,600	1968
8	10	0.1	0.3	12,500	1125
9	10	0.1	0.45	4200	462
10	25	10	0.15	115,600	6936
11	25	10	0.3	65,600	4592
12	25	10	0.45	22,800	2052
13	25	1	0.15	52,300	4184
14	25	1	0.3	18,060	1625
15	25	1	0.45	5840	642
16	25	0.1	0.15	9400	940
17	25	0.1	0.3	3120	374
18	25	0.1	0.45	1050	136
19	40	10	0.15	42,200	3798
20	40	10	0.3	18,800	1880
21	40	10	0.45	6650	731
22	40	1	0.15	12,200	1342
23	40	1	0.3	4250	510
24	40	1	0.45	1120	156
25	40	0.1	0.15	1850	240
26	40	0.1	0.3	860	129
27	40	0.1	0.45	120	22

3.3.2 Mechanisms Governing the Evolution of Cumulative Displacement and Sensitivity Analysis of Key Parameters

As illustrated in Figs. 5–7, the microscopic regulatory mechanisms and macroscopic mechanical responses of the interlayer displacement evolution in the 'SMA-13 + epoxy resin + steel plate' composite system are demonstrated under the influence of temperature, loading frequency and stress levels, respectively. As illustrated in Fig. 5, the evolution of shear displacement is observed at varying temperatures under a stress level of 0.3 S and a frequency of 1 Hz.

As the ambient temperature rises from 10°C to 40°C, the cumulative interlaminar displacement curve exhibited a significant overall upward shift, and the linear slope increased upon entering the second stage. At a temperature of 10°C, the interface demonstrated high stiffness, with displacement during the stable growth phase remaining at a minimal level throughout, and the ultimate failure displacement measuring approximately 5 mm. However, when the temperature rises to 40°C, the cumulative deformation for the same percentage of service life experienced a substantial increase, the ultimate displacement surged to over 7 mm, and the service life percentage at which the third stage commences was advanced from 90% to approximately 80%. This is attributable to the combination of two factors: firstly, the viscous softening of the bituminous binder at elevated temperatures, and secondly, the rheological properties of the epoxy interface. The consequence of these phenomena is a precipitous decline in the system's resistance to shear displacement. This phenomenon has been shown to not only enhance molecular slippage but also lead to a significant accumulation of residual deformation at the interface under cyclic loading.

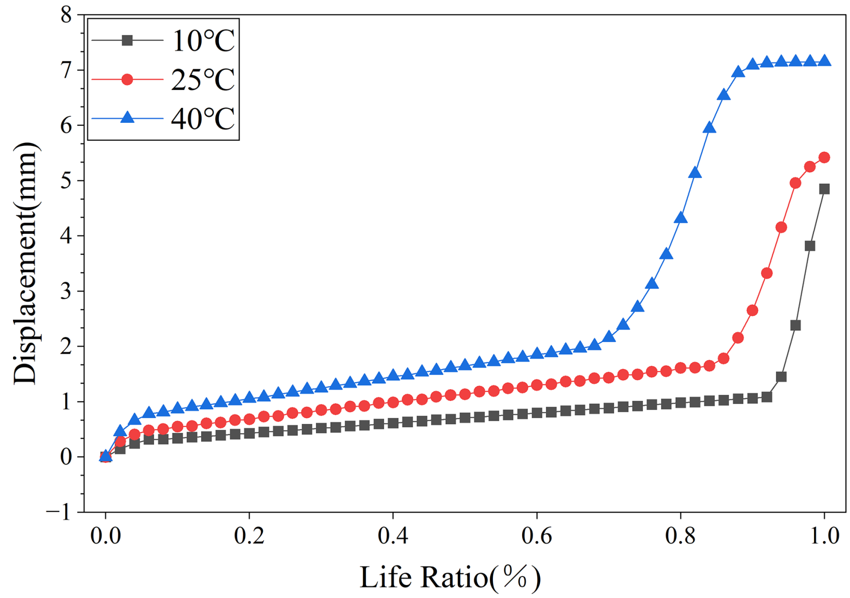

Figure 5: Effect of different temperatures on the evolution of cumulative interlayer shear displacement.

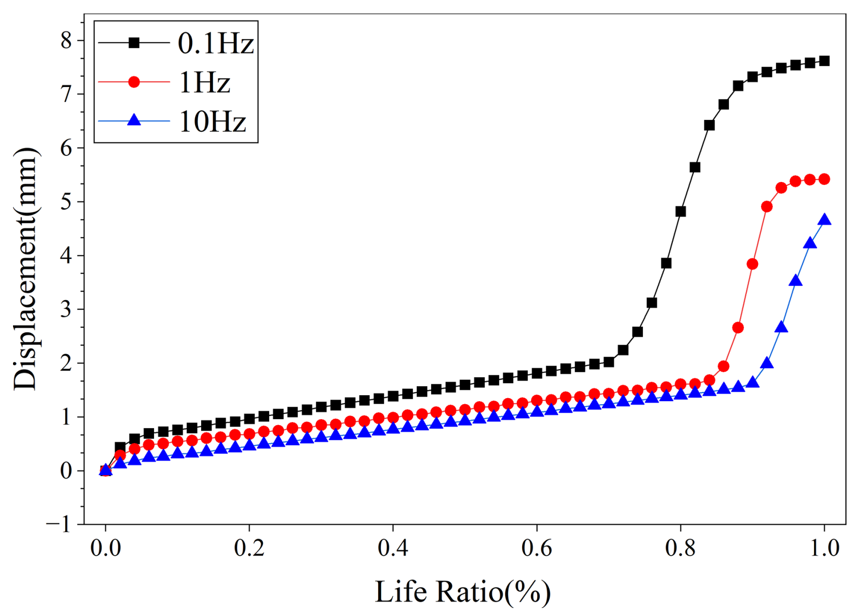

Figure 6: Effect of different loading frequencies on the evolution of cumulative interlaminar shear displacement.

The loading frequency is capable of simulating a range of vehicle speeds and exerts a substantial influence on the progression of interlayer fatigue. As illustrated in Fig. 6, the effect of varying frequencies on the cumulative displacement curve is demonstrated under conditions of 25°C and 0.3 S. The results indicated that as the loading frequency increased from 0.1 to 10 Hz, the cumulative shear displacement curve exhibited a marked downward shift, and the rate of acceleration towards instability in the third stage became increasingly steep. It has been demonstrated that, under low-frequency loading at 0.1 Hz, the duration of each load application is increased, resulting in a more pronounced accumulation of viscoelastic creep in the interface layer. The cumulative displacement was at its maximum, and the slope of the second stage was found to be the steepest. This indicates that low-frequency, slow-speed driving causes far greater damage to the shear fatigue of the steel bridge deck interlayers than high-frequency (10 Hz) rapid driving.

As illustrated in Fig. 7, the displacement curves demonstrate distinct characteristics at varying stress levels, operating under conditions of 25°C and 1 Hz. As the SSR increased from 0.15 to 0.45 S, the magnitude of the displacement jump in the first stage increased, and the damage accumulation rate in the second stage also increased exponentially. At an extremely elevated stress ratio of 0.45 S, the material's capacity to recover from deformation was markedly impeded, resulting in the onset of cracks entering an exceedingly unstable state of accelerated propagation, consequently precipitating a pronounced decline in overall fatigue life. Conversely, at a low stress ratio of 0.15 S, the curve manifested an exceptionally protracted period of stable growth with a slope that approaches zero. This finding suggested the presence of a strict power-law relationship between the stress level and the interlaminar fatigue life. This relationship indicates that a minor increase in stress can result in a substantial decrease in life expectancy.

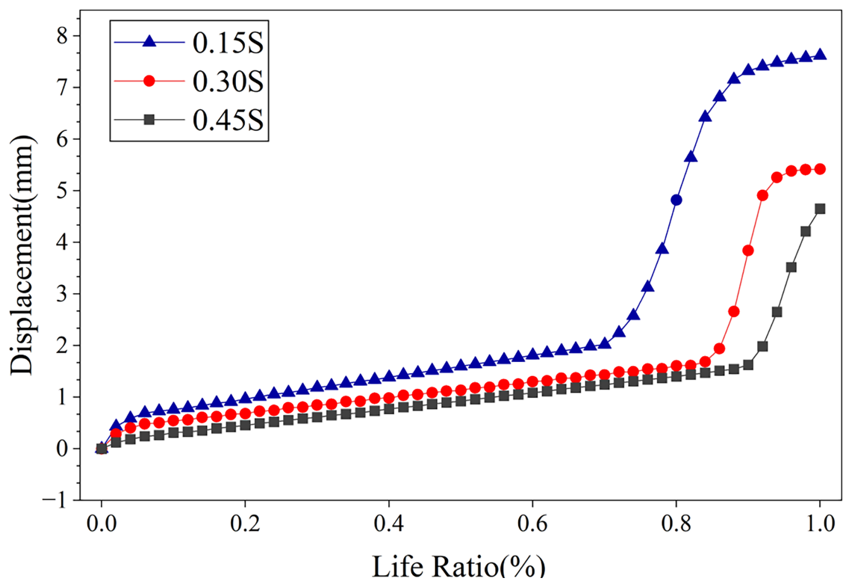

Figure 7: The effect of different stress levels on the evolution of cumulative interlaminar shear displacement.

As shown by the standard deviation σ in Table 4, the coefficient of variation tended to increase as the absolute value of N_f decreased. This finding suggested that interlaminar failure was characterised by increased randomness and suddenness under conditions of high temperature and heavy load. In order to provide further quantitative verification of the significance and hierarchical relationships of the various influencing factors from a statistical perspective, this study performed a one-way analysis of variance (ANOVA) on the experimental results using SPSS software. The statistical analysis yielded F-values of 145.2 ($p < 0.001$), 82.6 ($p < 0.001$), and 45.3 ($p < 0.001$), respectively, for the temperature variable, frequency, and stress level. Given that the p-values for all three factors were found to be significantly below the 0.05 level of significance, it can be deduced that all three variables exerted a substantial effect on fatigue life. Of greater significance is the finding that, based on the absolute magnitude of the F-values, this study rigorously verified from a statistical perspective that the order of sensitivity is as follows: ambient temperature > frequency (vehicle speed) > stress level (load weight).

3.4 Full-Factor Fatigue Life Prediction Model and Validation of Applicability

3.4.1 Development of the Predictive Model

The present study has developed a multi-factor fatigue life prediction model using the stress ratio *SSR*, loading frequency f and temperature T as independent variables, drawing on the phenomenological theory of fatigue. Its general mathematical expression is shown in Eq. (1):

$$N_f = k \cdot (SSR)^{-n_1} \cdot f^{n_2} \cdot 10^{aT} \tag{1}$$

In the given equation, the material constant k is represented by the first term. The stress sensitivity coefficient n_1 is denoted by the second term. The frequency correction coefficient n_2 is represented by the third term. The temperature influence factor α is denoted by the fourth term. Utilising the 27 sets of full-factor test data presented in Table 4, Eq. (1) was log-linearised, and a multiple linear regression analysis was conducted employing the least squares method. The results of the fitted parameters are displayed in Table 5, and the final prediction equation for the inter-slab shear fatigue life of long-span steel bridges is given by Eq. (2).

$$N_f = 2.85 \times 10^6 \cdot (SSR)^{-2.143} \cdot f^{0.685} \cdot 10^{-0.038T} \tag{2}$$

The regression results indicate that the coefficient of determination R^2 is 0.962, suggesting that the model provides a highly satisfactory explanation of the variation in the experimental data. The stress ratio exponent $n_1 = -2.143$ indicates that fatigue life is extremely sensitive to stress levels, exhibiting a rapid decline following a negative power law. The frequency exponent $n_2 = 0.685$ confirms the positive effect of high frequency (high speed) on extending fatigue life, reflecting the work-hardening effect of the material. The temperature coefficient $\alpha = -0.03$; this negative value quantitatively confirms the adverse effect of temperature increase on fatigue life, with life decreasing to approximately 40% of the original value for every 10°C rise in temperature.

Table 5: Fitted values for each parameter.

Parameters	k	n_1	n_2	α	**Correlation Coefficient R^2**
Fitted value	2.85×10^6	2.143	0.685	−0.038	0.962

3.4.2 Verification of Model Reliability

Fig. 8 presents a scatter plot that compared the measured service life from 27 sets of experiments with the model-predicted service life. As can be seen from the figure, all data points were closely clustered around the 45° standard isocline, with no obvious outliers. This demonstrated that the model exhibited extremely high predictive accuracy within the temperature range of 10°C–40°C and under various dynamic load combinations. The high correlation ($R^2 = 0.962$) demonstrated by this model was primarily based on the existing in-house laboratory dataset; independent external validation datasets had not yet been incorporated, nor has systematic K-fold cross-validation been conducted. Consequently, the model's robustness and generalisability when applied to different gradation types or binder systems must be verified in subsequent studies.

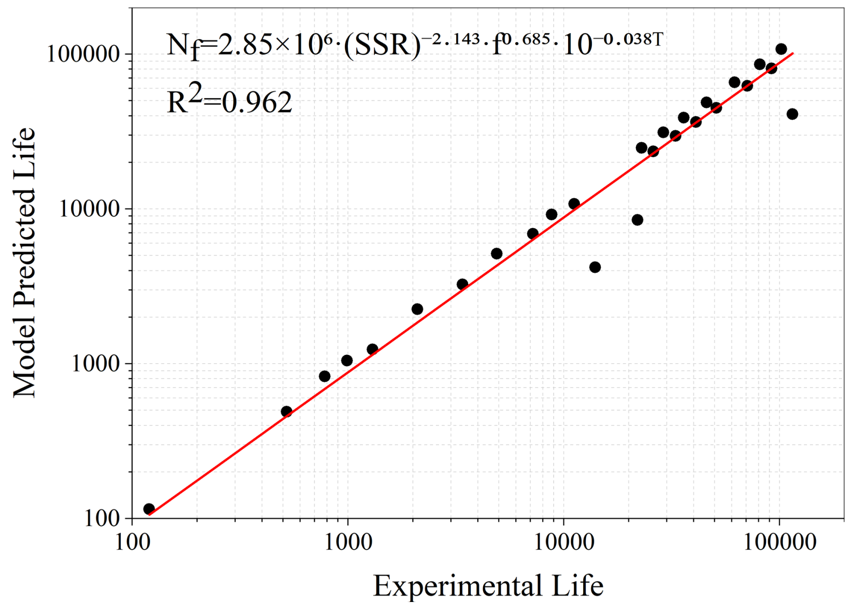

Figure 8: Scatter plot comparing measured lifespan with model-predicted lifespan.

4 Conclusion

The present paper sets out to present static direct shear and full-factor dynamic shear fatigue tests conducted on composite pavement systems for long-span steel bridges. In addition, it provided an in-depth investigation into the mechanism of interface damage evolution under the coupled action of multiple factors. The findings suggested that the shear strength of the epoxy resin bonding layer exhibited an initial increase, followed by a subsequent decrease, in accordance with the quantity of spray applied; the optimal spray application rate was determined to be 1.5 kg/m^2, at which point mechanical interlocking and chemical adhesion at the interface were achieved to the greatest extent. Furthermore, the interfacial shear strength demonstrated considerable temperature sensitivity; when the temperature rose from 10°C to 40°C, the shear strength decreased by 70%, and the failure mode transitioned from brittle fracture to ductile creep. In circumstances of dynamic loading, the cumulative interlaminar shear displacement typically evolves through three distinct stages, characterised by 'initial compaction—steady growth—accelerated failure'. The employment of the geometric tangent method in defining the fatigue life N_f was an effective strategy for mitigating errors arising from late-stage instability, thereby ensuring the accurate reflection of the true fatigue resistance of the interface. Interlayer fatigue life demonstrated extreme sensitivity to environmental and loading conditions, with the accelerating effects of various factors on fatigue damage ranked as follows: ambient temperature > loading frequency > stress ratio. It was demonstrated that elevated temperatures resulted in a substantial decrease in material modulus. Furthermore, low-frequency loading has been shown to intensify the accumulation of creep damage under single-pulse loading conditions. In the context of extreme coupled conditions, characterised by elevated temperatures (40°C), low frequencies (0.1 Hz) and elevated stress ratios, the fatigue life of the interface demonstrated an exponential decline. This observation signified that the convergence of high temperature, low speed and substantial loading constituted a high-risk critical condition, with the potential to induce interlayer slippage defects in steel bridge deck pavements. The establishment of a multivariate non-linear fatigue life prediction model was predicated on two fundamental concepts. The viscoelastic characteristics of polymeric materials must be taken into consideration in conjunction with the established laws governing fatigue damage evolution. The model must comprehensively account for temperature (T), frequency (f) and shear stress ratio (SSR). The regression results indicate that the model demonstrates a high degree of accuracy (R^2 = 0.962), with a reasonable distribution of residuals between measured and predicted values. However, it should be noted that the conclusions of this study are primarily based on small composite specimens tested under ideal indoor conditions; laboratory testing has inherent limitations in simulating the complex boundary conditions found on bridge decks, such as actual local deflections and wind-induced vibrations. It is imperative that future research endeavours promptly establish independent field validation datasets and undertake long-term performance monitoring based on actual bridge projects. This will facilitate the validation and refinement of service life prediction models, thereby enhancing their robustness in practical engineering evaluations.

Acknowledgement: Not applicable.

Funding Statement: The authors received no specific funding for this study.

Author Contributions: The authors confirm contribution to the paper as follows: Conceptualization, Jiyi Li and Xinxin Cao; methodology, Jiyi Li; software, Zongqi Xiong; validation, Jiyi Li, Zongqi Xiong and Xinxin Cao; formal analysis, Jiyi Li; investigation, Zongqi Xiong; resources, Xinxin Cao; data curation, Zongqi Xiong; writing—original draft preparation, Jiyi Li; writing—review and editing, Xinxin Cao; visualization, Zongqi Xiong; supervision, Xinxin Cao. All authors reviewed and approved the final version of the manuscript.

Availability of Data and Materials: The data that support the findings of this study are available from the corresponding author, Xinxin Cao, upon reasonable request.

Ethics Approval: Not applicable.

Conflicts of Interest: Jiyi Li and Zongqi Xiong are full-time employees of their respective affiliated institutions, which also provided funding for this study. This paper is based on the research project led by Xinxin Cao, and both Li and Xiong participated in the study. The authors affirm that there are no other financial or personal conflicts of interest that could have influenced the work reported in this manuscript.

References

1. Chen X, Huang W, Yang J, Wang D. Principles of designing asphalt pavement for orthotropic steel bridge decks. In: Material design, construction, maintenance, and testing of pavements. Reston, VA, USA: American Society of Civil Engineers; 2009. p. 45–154. doi:10.1061/41045(352)23.
2. Abdelbaset H, Zhu Z. Behavior and fatigue life assessment of orthotropic steel decks: a state-of-the-art-review. Structures. 2024;60:105957. doi:10.1016/j.istruc.2024.105957.
3. Backer HD. Orthotropic steel decks. In: Innovative bridge design handbook. Amsterdam, The Netherlands: Elsevier; 2022. p. 711–27. doi:10.1016/b978-0-12-823550-8.00028-7.
4. Zhu Z, Zhu R, Xiang Z. A review on behavior and fatigue performance of orthotropic steel–UHPC composite deck. Buildings. 2023;13(8):1906. doi:10.3390/buildings13081906.
5. Siwowski T, Kulpa M, Janas L. Remaining fatigue life prediction of welded details in an orthotropic steel bridge deck. J Bridge Eng. 2019;24(12):05019013. doi:10.1061/(asce)be.1943-5592.0001490.
6. Wang D, Tan B, Wang X, Zhang Z. Experimental study and numerical simulation of temperature gradient effect for steel-concrete composite bridge deck. Meas Control. 2021;54(5–6):681–91. doi:10.1177/00202940211007166.
7. Haibara Y, Ge H, Sun J. Materials optimization and service performance evaluation of a novel steel bridge deck pavement structure: a case study. Appl Sci. 2023;13(10):5930. doi:10.3390/app13105930.
8. Yang K, Li R, Yu Y, Pei J, Liu T. Evaluation of interlayer stability in asphalt pavements based on shear fatigue property. Constr Build Mater. 2020;258:119628. doi:10.1016/j.conbuildmat.2020.119628.
9. Xu Y, Lv X, Ma C, Liang F, Qi J, Chou Z, et al. Shear fatigue performance of epoxy resin waterproof adhesive layer on steel bridge deck pavement. Front Mater. 2021;7:618073. doi:10.3389/fmats.2020.618073.

10. Wang X, Zhang C, Sun R. Response analysis of orthotropic steel deck pavement based on interlayer contact bonding condition. Sci Rep. 2021;11:23692. doi:10.1038/s41598-021-03137-7.
11. Chen W, Hui B, Rahman A. Interlayer shear characteristics of bridge deck pavement through experimental and numerical analysis. Materials. 2022;15(19):7001. doi:10.3390/ma15197001.
12. Zhu C, Li W, Wang H. Analysis of interlayer crack propagation and strength prediction of steel bridge deck asphalt pavement based on extended finite element method and cohesive zone model (XFEM–CZM) coupling. Coatings. 2023;13(11):1973. doi:10.3390/coatings13111973.
13. Diakhate M, Phelipot A, Millien A, Petit C. Shear fatigue behaviour of tack coats in pavements. Road Mater Pavement Des. 2006;7(2):201–22. doi:10.1080/14680629.2006.9690033.
14. Liu Y, Qian Z, Yin Y, Ren H. Investigation on interlayer behaviors of a double-layered heterogeneous asphalt pavement structure for steel bridge deck. J Mater Civ Eng. 2022;34(5):04022062. doi:10.1061/(asce)mt.1943-5533.0004206.
15. He Z, Pei D, Xu L, Peng R, Zhang O, Tang J, et al. Toward sustainable thermosets: advances in toughening and degradation strategies for epoxy resins. Cell Rep Phys Sci. 2025;6(10):102855. doi:10.1016/j.xcrp.2025.102855.
16. Bocci E, Graziani A, Canestrari F. Mechanical 3D characterization of epoxy asphalt concrete for pavement layers of orthotropic steel decks. Constr Build Mater. 2015;79:145–52. doi:10.1016/j.conbuildmat.2014.12.120.
17. Chen X, Chen Y, Ma T, Gu L, Shi S. Study on the performances of epoxy asphalt binders influenced by the dosage of epoxy resin and its application to steel bridge deck pavement. Constr Build Mater. 2024;432:136683. doi:10.1016/j.conbuildmat.2024.136683.
18. Zhou L, Zhang D, Li X, Gao Z, Chen Q, Wang C. Overview: application of resin waterproof adhesive materials in bridge deck pavement in China. Adv Civ Eng. 2022;2022:2320374. doi:10.1155/2022/2320374.
19. Yu H, Feng X, Ge J, Qian G, Zhang C, Zhong Y, et al. Evaluation of the developed and performance of epoxy resin bonding materials for steel bridge deck pavement layers. Constr Build Mater. 2024;455:139155. doi:10.1016/j.conbuildmat.2024.139155.
20. Demiral M. Strength in adhesion: a multi-mechanics review covering tensile, shear, fracture, fatigue, creep, and impact behavior of polymer bonding in composites. Polymers. 2025;17(19):2600. doi:10.3390/polym17192600.
21. Zhao M, Huang W, Jin F, Zhu B, Zhang G, Ding Q, et al. Investigation of surface treatments and bonding materials on static and dynamic shear bonding performance at UHPC-SMA bridge deck interfaces. Constr Build Mater. 2026;519:145892. doi:10.1016/j.conbuildmat.2026.145892.
22. Guan YS, Han C, Li MJ, Yan L. Performance of modified epoxy resin waterproof adhesive layer on cement concrete bridge surface. J Build Mater. 2013;16(5):894–8. doi:10.3969/j.issn.1007-9629.2013.05.027.
23. Rahman A, Huang H, Ai C, Ding H, Xin C, Lu Y. Fatigue performance of interface bonding between asphalt pavement layers using four-point shear test set-up. Int J Fatigue. 2019;121:181–90. doi:10.1016/j.ijfatigue.2018.12.018.
24. Atul Narayan SP, Little DN, Rajagopal KR. Incorporating disparity in temperature sensitivity of asphalt binders into high-temperature specifications. J Mater Civ Eng. 2019;31:04018343. doi:10.1061/(asce)mt.1943-5533.0002534.
25. Chen X, Lin Z, Ma T, Gu L, Chen Y, Shi S. Study on hot-mix epoxy resin based on glass transition temperature and its application for steel bridge deck pavement. J Mater Civ Eng. 2024;36(8):04024239. doi:10.1061/jmcee7.mteng-17644.
26. Jin T, Liu L, Yang R, Sun L, Yuan J. Investigation of interlayer bonding performance between asphalt concrete overlay and Portland cement concrete using inclined shear fatigue test. Constr Build Mater. 2023;400:132681. doi:10.1016/j.conbuildmat.2023.132681.
27. Zhang S, Zhang H, Zhou M. Investigation on the high-temperature stability and fatigue behavior of cold mixed epoxy asphalt mixture with different gradations. Case Stud Constr Mater. 2024;20:e02694. doi:10.1016/j.cscm.2023.e02694.
28. Xu X, Yang X, Huang W, Xiang H, Yang W. New damage evolution law for steel-asphalt concrete composite pavement considering wheel load and temperature variation. Materials. 2019;12(22):3723. doi:10.3390/ma12223723.
29. Zhou F, Scullion T, Sun L. Verification and modeling of three-stage permanent deformation behavior of asphalt mixes. J Transp Eng. 2004;130(4):486–94. doi:10.1061/(asce)0733-947x(2004)130:.
30. Yuan MM, Zhang XN, Chen WQ, Zhang SX. Ratio of dissipated energy change-based failure criteria of asphalt mixtures. Res J Appl Sci Eng Technol. 2013;6(14):2514–9. doi:10.19026/rjaset.6.3731.